

Understanding the Chemistry of the Rocks at Jezero crater, Mars, through the Combined Use of SuperCam Spectroscopic and Optical Techniques

Juan Manuel Madariaga^{1,1,1}, Roger Wiens^{2,2,2}, Gorka Arana^{3,3,3}, Violaine Sautter^{4,4,4}, Karim Benzerara^{5,5,5}, Arya Udry^{6,6,6}, Olivier Beyssac^{7,7,7}, Lucia Mandon^{8,8,8}, Olivier Gasnault^{9,9,9}, Jeffrey Johnson^{10,10,10}, Ann Ollila^{2,2,2}, Kepa Castro^{3,3,3}, Agnes Cousin^{11,11,11}, Sylvestre Maurice^{9,9,9}, Samuel Clegg^{2,2,2}, Ryan Anderson^{12,12,12}, Tanja Bosak^{13,13,13}, Pierre Beck^{14,14,14}, Thierry Fouchet^{8,8,8}, Svetlana Shkolyar^{15,15,15}, Edward Cloutis^{16,16,16}, Cathy Quantin-Nataf^{17,17,17}, Imanol Torre Fernandez^{3,3,3}, Clément Royer^{8,8,8}, Chip Legett^{2,2,2}, and Paolo Pilleri^{9,9,9}

¹University of the Basque Country

²Los Alamos National Laboratory

³Universidad del País Vasco / Euskal Herriko Unibertsitatea

⁴MNHN National Museum of Natural History Paris

⁵Institut de Minéralogie, de Physique des Matériaux et de Cosmochimie, UPMC / CNRS / MNHN / IRD

⁶University of Nevada Las Vegas

⁷IMPMC Institut de Minéralogie et de Physique des Milieux Condensés

⁸LESIA, Observatoire de Paris, Université PSL, CNRS, Sorbonne Université, Université de Paris

⁹IRAP, CNRS, Université de Toulouse, UPS-OMP

¹⁰Johns Hopkins University Applied Physics Laboratory

¹¹Institut de Recherche en Astrophysique et Planétologie (IRAP)

¹²United States Geological Survey

¹³MIT, Earth, Atmospheric and Planetary Sciences

¹⁴University Joseph Fourier Grenoble

¹⁵ASU

¹⁶University of Winnipeg

¹⁷Université de Lyon, UCBL, ENSL, CNRS, LGL-TPE

November 30, 2022

Abstract

The SuperCam instrument onboard Perseverance rover has remote imaging (RMI), VISIR, LIBS, Raman and Time-Resolved Luminescence (TRL) capabilities. RMI images of the rocks at the Octavia Butler landing site have revealed important granular texture diversities. VISIR raster point observations have revealed important differences in the 2.10-2.50 μm infrared range (metal-hydroxides); many include water features at 1.40 ± 0.04 and 1.92 ± 0.02 μm [1]. LIBS observations on the same points analyzed by VISIR revealed important differences in the concentrations of major elements, suggesting mineral grain sizes larger

than the laser beam (300-500 μm). LIBS and VISIR show coherent results in some rock surfaces that are consistent with an oxy-hydroxide (e.g., ferrihydrite) [1]. LIBS elemental compositions are consistent with pyroxenes, feldspars, and more often feldspar-like glass, often enriched in silica. Olivine compositions [1, 2] have been observed so far in LIBS data (up to Sol 140) exclusively in rounded regolith pebbles. They have not yet been observed in the rocks themselves, which are MgO-poor compared to regolith and are consistent with FeO bearing pyroxenes (e.g., hedenbergite, ferrosilite). A 3x3 LIBS and VISIR raster (9x9 mm) acquired on a low-standing rock on sol 90 exemplifies these findings. A dark L-shaped filled void sampled by points 1 and 2 with possible ferrihydrite (H seen in LIBS and VISIR spectra). Point 5 contains abundant silica and alkali elements but is Al-depleted relative to feldspars, consistent with dacitic glass composition. Point 7 has TiO_2 content consistent with ilmenite. Comparisons to (igneous) Martian meteorites are potentially useful, e.g. [3], to explain the presence of several minerals, although most Martian meteorites are olivine-rich, e.g., more mafic than the rocks at the landing site. In summary, the bedrock at Octavia Butler landing site can be interpreted as showing evidence for relatively coarse-grained weathered pyroxenes, iron and titanium oxides and feldspars, while the local soil contains pebbles from a different source (richer in MgO) incorporating olivine grains. References: [1] Mandon et al. 2021 Fall AGU, New Orleans, LA, 13-17 Dec. ; [2] Beyssac et al. 2021 Fall AGU, New Orleans, LA, 13-17 Dec. ; [3] Garcia-Florentino et al.(2021), *Talanta*, 224, 121863.

Understanding the chemistry of the rocks at Jezero crater, Mars, through the combined use of SuperCam spectroscopic and optical techniques

J. M. Madariaga^{1*}, R. C. Wiens², G. Arana¹, V. Sautter³, K. Benzerara³, A. Udry⁴, O. Beyssac³, L. Mandon⁵, O. Gasnault⁶, J.R. Johnson⁷, A. M. Ollila², K. Castro¹, A. Cousin⁶, S. Maurice⁶, S. Clegg², R. B. Anderson⁸, T. Bosak⁹, P. Beck¹⁰, T. Fouchet⁵, S. Shkolyar¹¹, E. Cloutis¹², C. Quantin-Nataf¹³, I. Torre-Fdez¹, C. Royer⁵, C. Legett², P. Pilleri⁶, and the SuperCam team

¹University of the Basque Country (UPV/EHU), Bilbao, Spain; ²Los Alamos National Laboratory, Los Alamos, NM, USA; ³IMPMC, Museum National d'Histoire Naturelle, CNRS, Sorbonne Université, Paris, France; ⁴University of Nevada, Las Vegas, NV, USA; ⁵LESIA, Observatoire de Paris, Université PSL, CNRS, Sorbonne Université, Meudon, France; ⁶IRAP, CNRS, Université de Toulouse, UPS-OMP, Toulouse, France; ⁷John Hopkins University Applied Physics Laboratory, Laurel, MD, USA; ⁸U.S. Geological Survey, Flagstaff, AZ, USA; ⁹Dept. Earth, Atmospheric and Planetary Science, MIT, MA, USA; ¹⁰Université Grenoble-Alpes, CNRS, IPAG, UMR 5274, Grenoble, France; ¹¹ NASA Goddard Space Flight Center, MD, USA; ¹²University of Winnipeg, Winnipeg, Canada; ¹³Université de Lyon, LGL-TPE UCBL, ENSL, CNRS Lyon, France; (*) juanmanuel.madariaga@ehu.eus

INTRODUCTION

The SuperCam instrument onboard Perseverance rover has remote imaging (RMI), VISIR, LIBS, Raman and Time-Resolved Luminescence (TRL) capabilities. Once the post-landing tests on all elements and spectrometers of SuperCam were completed, the science activities started with the analysis of rocks, pebbles, and soils, first at the Octavia E. Butler (OEB) landing site and then in the Crater Floor Fractured Rough (Cf-fr) unit (Sol <170), in the Artuby ridge (170≤Sol≤201), and currently in the Seitah unit (Sol >201), as depicted in Figure 1 for the Sols until Conjunction.

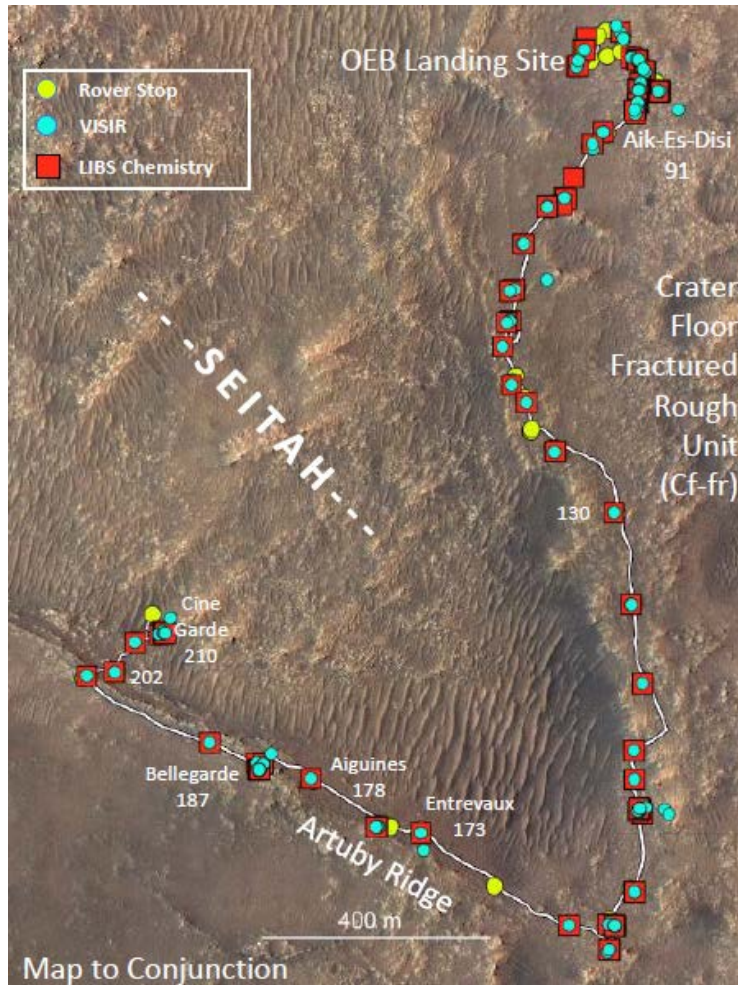


Figure 1.- Traverse of the Perseverance rover indicating the sites where SuperCam performed science activities until Conjunction. Since then it has collected two samples of Seitah.

IMAGE AND SPECTROSCOPIC OBSERVATIONS

RMI images of the rocks at the OEB landing site and the Cf-fr unit, both High-Standing (Cf-Fr Hi) and Low-standing (Cf-fr Lo) rocks (Figure 2), have revealed important granular texture diversities. VISIR raster point observations have revealed important differences in the 2.10-2.50 μm infrared range (metal-hydroxides); many include water features at 1.40 ± 0.04 and 1.92 ± 0.02 μm [1] suggesting the presence of alteration minerals. LIBS observations on the same points analyzed by VISIR revealed important differences in the concentrations of major elements, suggesting mineral grain sizes larger than the laser beam (300-500 μm); moreover, the sum of the 8 major elements (%SiO₂, %TiO₂, %Al₂O₃, %FeOT, %MgO, %CaO, %Na₂O, and %K₂O) quantified from LIBS spectra never reached 100%, suggesting the presence of alteration phases.

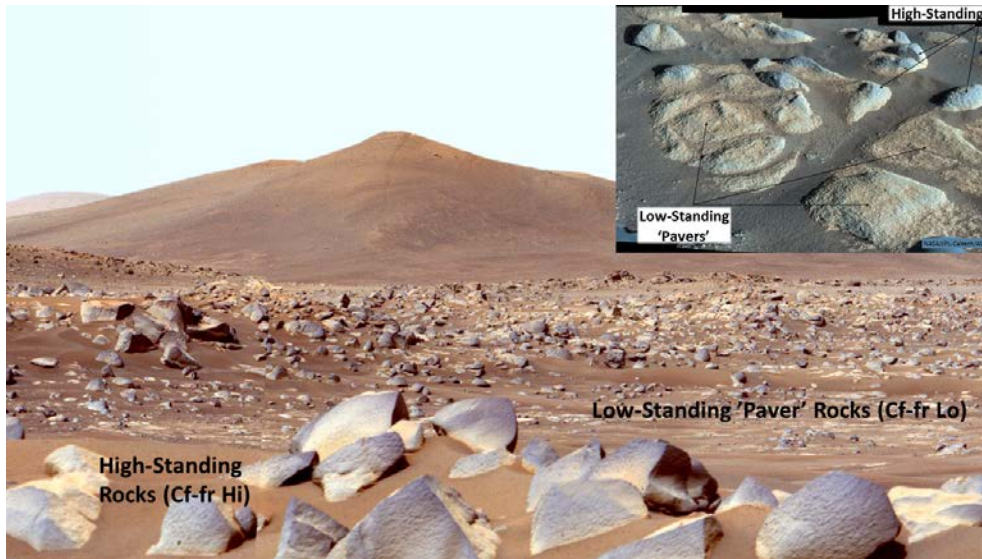


Figure 2.- High-Standing (Cf-Fr Hi) and Low-standing (Cf-fr Lo) rocks at the Crater Floor Fracture Rough unit. The Cf-fr Hi are darker rocks while the Cf-fr Lo are paver rocks.

LIBS elemental compositions of rocks at the OEB landing site and the Cf-Fr unit are consistent with pyroxenes, feldspars, and more often feldspar-like glass, often enriched in silica. Olivine compositions [1, 2] have been observed so far in LIBS data (up to Sol 140) exclusively in rounded regolith pebbles. They were not observed in the Cf-fr rocks themselves, which are MgO-poor compared to regolith and are consistent with FeO bearing pyroxenes (e.g., hedenbergite, ferrosilite). Figure 3 shows the dispersion obtained from those rock targets, with observations close to andesine and enstatite endmembers and intermediate situations close to diopside (the black points belong to the pyroxenes and olivine present in the calibration target of SuperCam).

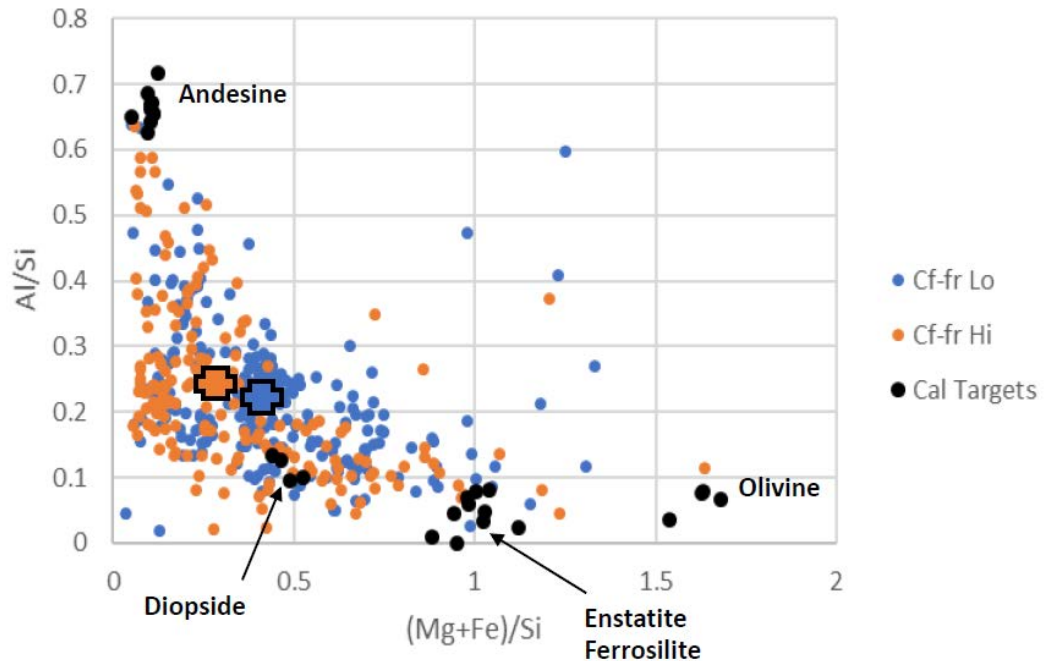


Figure 3.- Diversity of the Cf-Fr Hi and Cf-fr Lo rocks in comparison with the pyroxene-olivine samples included in the calibration target of SuperCam. Crosses are the mean value for each rock type.

A 3x3 LIBS and VISIR raster (9x9 mm) acquired on the Tostid_tsaadah low-standing rock on sol 90 exemplifies these findings. Figure 4 shows the geologic context of rock containing the Tostid_tsaadah target (NavCam image), and the proximity (RMI image) and detail of the 9 points of the raster. Table 1 summarizes the %MeO values, with their uncertainties (standard deviations of 25 spectra at each observation point), for the 9 observations on this target.

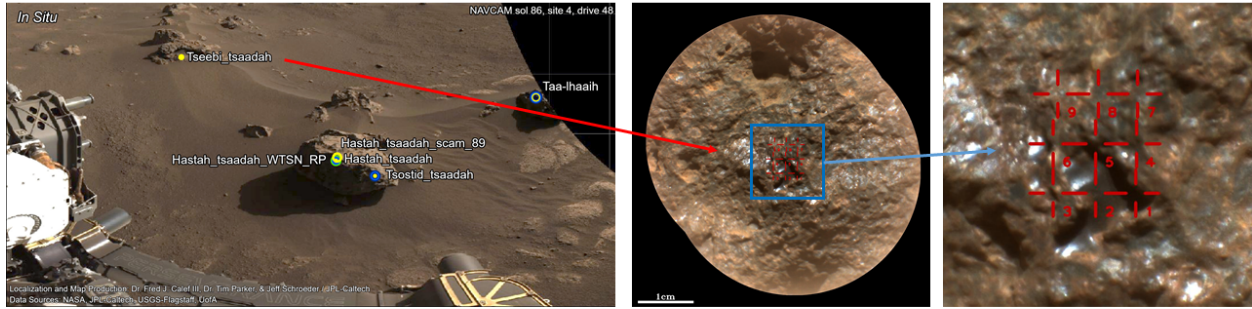


Figure 4.- Long distance, proximity and near microscopic detail of the Tostid_tsaadah target

Table 1.- Percent of Metal-Oxide units for concentrations and standard deviation values of Tostid_tsaadah low-standing rock, Sol 90

Point	SiO ₂	SiO ₂ stdev	TiO ₂	TiO ₂ stdev	Al ₂ O ₃	Al ₂ O ₃ stdev	FeOT	FeOT stdev	MgO	MgO stdev	CaO	CaO tdev	Na ₂ O	Na ₂ O stdev	K ₂ O	K ₂ O stdev	Total
1	1.07	1.85	0.06	0.01	1.61	1.62	80.56	3.05	2.52	0.93	0.66	0.50	1.02	0.11	0.51	0.63	88.01
2	3.98	1.85	0.07	0.01	2.12	0.83	82.85	2.68	3.66	0.92	1.24	0.71	1.32	0.07	0.00	0.08	95.24
3	26.63	8.54	0.07	0.02	3.79	1.57	49.15	13.27	2.72	0.85	2.03	0.61	1.66	0.18	1.00	0.57	87.05
4	51.13	1.81	0.11	0.01	3.08	1.01	40.06	5.12	0.86	0.48	1.57	0.39	1.64	0.32	0.30	0.29	98.75
5	62.50	1.29	0.18	0.04	12.30	0.67	2.42	0.87	0.69	0.16	1.19	0.28	4.31	0.28	4.51	0.48	88.10
6	45.04	3.13	0.03	0.01	5.98	1.11	35.73	4.93	3.22	1.46	1.86	0.54	3.96	0.26	1.26	0.52	97.08
7	23.87	2.90	1.96	0.09	4.21	1.58	27.79	7.33	2.54	1.09	3.46	0.45	1.90	0.34	0.48	0.51	66.21
8	46.20	5.07	0.52	0.06	1.89	1.18	61.94	7.19	1.62	0.67	1.26	0.66	1.41	0.11	0.42	0.63	115.26
9	51.46	3.06	0.46	0.20	7.03	1.15	13.36	5.55	3.13	0.86	4.17	1.66	3.39	0.36	1.63	0.45	84.63

The dark L-shaped filled void, sampled by points 1 and 2, shows high H signal in LIBS, together with the highest concentration of Fe and the lowest of Si, and the VISIR spectra is consistent with ferrihydrite [1]. Point 5 contains abundant silica and alkali elements, with a molar ratio of Al/(Na+K) close to 1, consistent with albite in an amount of 64% of the total mass; the excess of silica could be consistent with dacitic glass composition. Point 7 has TiO₂ content consistent with ilmenite (the calibration underestimates Ti at high abundances).

The rocks analyzed along Artuby ridge (Fig. 1) started to show clear olivine signatures in the VISIR spectra, as depicted by the slope of the spectra in the 1.3-1.8 μm range. This was more evident when the rover left Artuby and started the Seitah campaign, as it can be observed in Figure 5 where the slope, in the 1.3-1.8 μm range, of the VISIR spectra collected from the beginning of the mission is plotted against the Sol numbers.

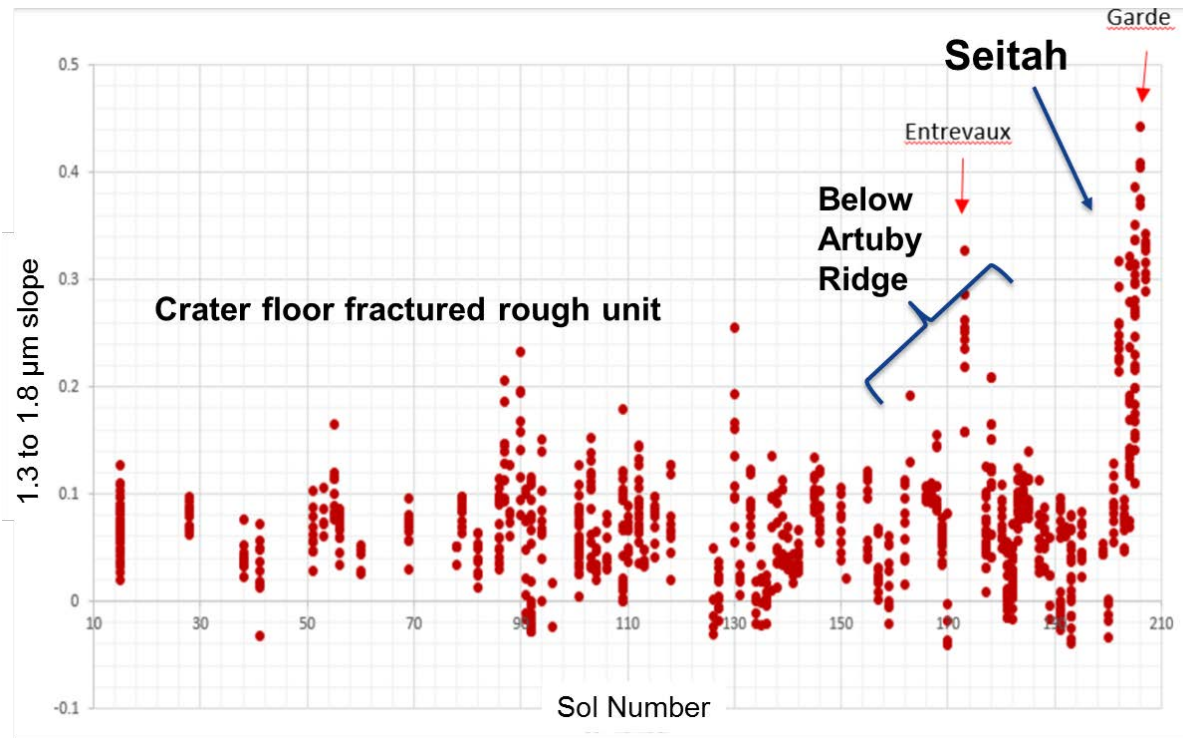


Figure 5.- Slope values in the 1.3-1.8 μm range of VISIR spectra collected until Sol 208

LIBS observations agree with VISIR data. Figure 6 shows the elemental abundances of Seitah rocks to be in the olivine range of the pyroxene-olivine diagram. Comparing the distribution of the rocks in the Cf-fr unit (Figure 3) and Artuby-Seitah (Figure 6), rocks are less felsic and more mafic as the rover traverses from OEB to Seitah. However, there are common rocks in all units, e.g. the rocks showing a distribution in the middle ($0.3 < (Mg+Fe)/Si < 0.7$) of the pyroxene-olivine diagram.

In contrast with this trend observed in the rocks, the small pebbles on top of the soil show a constant chemical and mineralogical composition. Figure 7 shows the fairly constant concentration of Si, Fe, Mg and Ca in 25 selected points on small pebbles distributed from Sol 72 until sol 236. The pebbles are composed of the same mixture of four minerals, albite, anorthite, diopside and olivine with slight differences in their relative amounts, with olivine as the most abundant (nearly 75%) of the mineral phases.

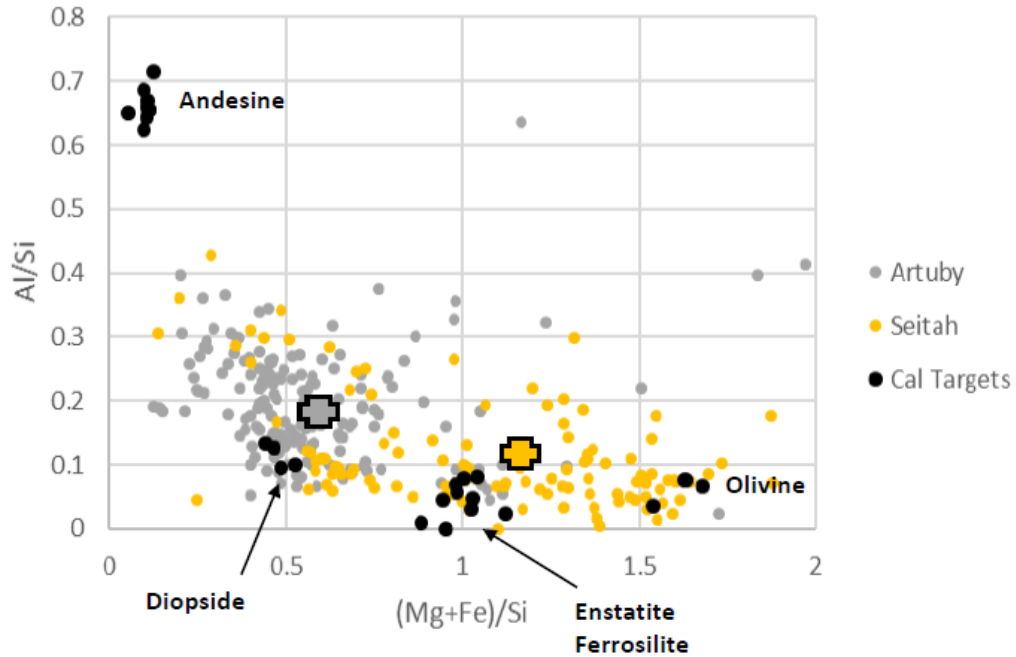


Figure 6.- Diversity of the Artuby and Seitah rocks in comparison with the pyroxene-olivine standards included in the calibration target of SuperCam. Crosses are the mean values for both regions.

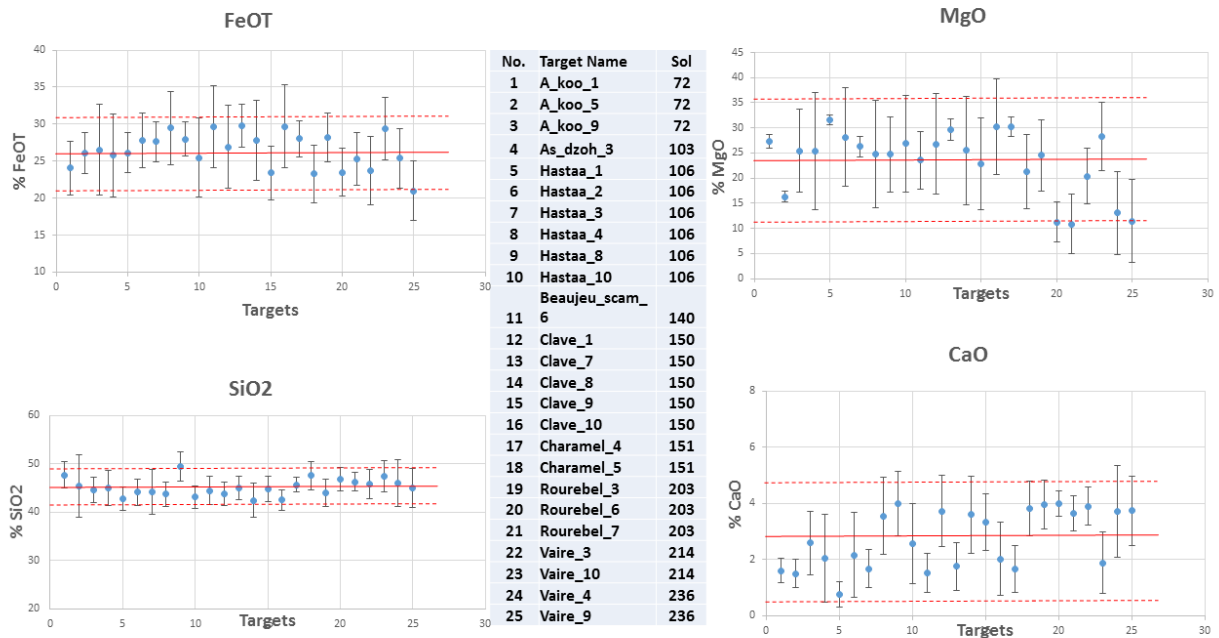


Figure 7.- Concentration of Si, Fe, Mg and Ca in 25 small pebbles deposited on top of soil surfaces from Sol 72 until Sol 236. The mean value and the ± 2 standard deviation uncertainty

boundary (dashed lines) cover all observed values. The whole FeOT belongs to olivine, while MgOH is split into olivine and diopside, and CaO into anorthite and diopside

CONCLUSIONS

Comparisons to (igneous) Martian meteorites are potentially useful, e.g. [3], to explain the presence of several minerals, although most Martian meteorites are pyroxene- and olivine-rich, e.g., more mafic than the rocks at the landing site but more similar to the rocks in Seitah. In summary, the bedrocks at Octavia Butler landing site and the Cf-fr unit can be interpreted as showing evidence for relatively coarse-grained weathered pyroxenes, iron and titanium oxides and feldspars, while the local soil contains pebbles from a different source (richer in MgO) incorporating olivine grains. Artuby can be considered a transition between Seitah and the Cf-fr units because the presence of olivine in the rocks increases and feldspar-plagioclase minerals decrease. The rocks in Seitah are rich in olivine, decreasing the relative amount of pyroxene and alumino-silicate phases. It is noteworthy that the small pebbles on top of the soils of Seitah and Cf-Fr units have nearly the same composition as Seitah rocks, with olivine in the range of 64-88%, pyroxene between 5 and 15% and feldspar-plagioclase in the range 14-21%.

References

- [1] Mandon et al. 2021 Fall AGU, New Orleans, LA, 13-17 Dec.
- [2] Beyssac et al. 2021 Fall AGU, New Orleans, LA, 13-17 Dec.
- [3] Garcia-Florentino et al. (2021), *Talanta*, **224**, 121863.